GEOPHYSICS, VOL. 66, NO. 1 (JANUARY-FEBRUARY 2001); P. 283–293, 11 FIGS., 1 TABLE.

Amplitude variations with offset of pressure-seal reflections

José M. Carcione*

ABSTRACT

Knowledge of pressure compartments is essential for identifying potential risks in advance of drilling and in understanding the mechanism of hydrocarbon trapping and migration. These compartments are bounded by pressure seals which, under certain conditions, can be detected and characterized with seismic reflection data. Use of prestack seismic data requires the analysis of reflections generated at the pressure seals, such as the top of a reservoir, rather than the properties of the rock volume. In this sense, amplitude variations with offset (AVO) techniques can be a good tool to obtain information from such pressure seals or pressure transition zones. In this work, I investigate the AVO response of compartment seals by analyzing the plane-wave reflection coefficients as a function of pore pressure (above and below the seal), incidence angle, and seal thickness. For the case investigated in this work (Berea sandstone with high gas saturation), the AVO effects are important at low effective pressures, that is, when the pore pressure approaches the confining pressure. In shale-free transition zones, the anomaly is, in general, negative, whereas in shale/sandstone sequences, the anomaly can be positive or negative depending on seal thickness and formation pressure. In terms of the four-category classification for AVO crossplotting, the *PP* anomalies are mainly class IV and class I.

INTRODUCTION

Pressure compartments are common in sedimentary basins (Chiarelli and Duffaud, 1980; Bradley and Powley, 1994; Law et al., 1998). Their knowledge is extremely important to the drilling engineer to prevent blowouts and/or lost circulations. Pressure compartments can be subdivided into two different classes: those created by disequilibrium compaction and characterized by large volumes of low permeability rock, and those bounded by seals, which are formed by a combination of low permeability effects (e.g., shales) and high capillarity pressure due to the interfacial tension between two fluids (Iverson et al., 1994).

Pressure compartments are bounded by pressure seals. Unlike pure capillary seals, which permit the flow of the wetting phase (brine), a pressure seal restricts both hydrocarbon and brine flow. Here, I consider a pressure compartment, surrounded by pressure seals, acting as a petroleum trapping mechanism. This compartment behaves as a closed hydraulic system, so the fluids within the system may be underpressured, normally pressured, or overpressured. In some cases, interbedded shale and sandstone layers act as a transition between normal and abnormal pressures (Bradley and Powley, 1994). Another proposed mechanism is the so-called vapor-lock pressure seal, where gas exsolution creates a relative permeability barrier that restricts upward flow (Benzing and Shook, 1996). In this case, the seal is associated with high pressure gradients within the sandstone. In some cases, the transition is very sharp, indicating a very thin seal compared to the vertical and lateral dimensions of the rock volume. This situation is also common in impermeable faults in relatively uniform shale-free sandstone lithologies (Heath et al., 1994).

Seismic data can be used to predict abnormal pore pressures in advance of drilling. In general, this prediction has been based on normal moveout (NMO) analysis (e.g., Bilgeri and Ademeno, 1982) and empirical models relating pore pressure to seismic properties. Louis and Asad (1994) used a modeling technique to analyze the amplitude variations with offset (AVO) of pressure seals. Acoustic synthetic seismograms based on well logs showed that a strong AVO effect is associated with steep pressure and velocity gradients.

In this work, I develop a model for relating pore pressure to the seismic properties of a closed rock volume (the compartment), and investigate the AVO response of pressure seals consisting of interbedded shale and sandstone units. The pressure model assumes that the pores are filled with oil, gas, and brine. Balancing volume fractions in the pore space yields the fluid saturations and also the porosity versus pore pressure [which is a function of the initial (hydrostatic) saturations and porosity]. Moreover, laboratory experiments on dry and saturated samples, for different confining and pore pressures, provide the rock moduli versus effective pressure. The AVO response

Manuscript received by the Editor April 19, 1999; revised manuscript received March 24, 2000.
*Osservatorio Geofisico Sperimentale, P.O. Box 2011, Opicina, 34016 Trieste, Italy. E-mail: jcarcione@ogs.trieste.it.

of the seal is obtained by computing the reflection coefficient of a set of transversely isotropic layers (the seal) embedded between two isotropic half-spaces (the rock units above and below the seal).

PRESSURE MODEL

First, I introduce some useful definitions about the different pressures considered in this work. *Pore pressure*, also known as formation pressure, is the in-situ pressure of the fluids in the pores. The pore pressure is equal to the *hydrostatic pressure* when the pore fluids only support the weight of the overlying pore fluids (mainly brine). The *lithostatic* or *confining pressure* is due to the weight of overlying sediments, including the pore fluids. In the absence of any state of stress in the rock, the pore pressure attains lithostatic pressure and the fluids support all the weight. However, fractures perpendicular to the minimum compressive stress direction appear for a given pore pressure, typically 70–90 % of the confining pressure. In this case, the fluid escapes from the pores, and pore pressure decreases. A rock is said to be overpressured when its pore pressure is significantly greater than hydrostatic pressure. The difference between pore pressure and hydrostatic pressure is called *differential pressure*. Acoustic and transport properties of rocks generally depend on *effective pressure*, a linear combination of pore and confining pressures [see equation (1)]. Various physical processes cause anomalous pressures on an underground fluid. The most common causes of overpressure are thermal expansion of water, compaction disequilibrium, and cracking (i.e., oil to gas conversion) (Mann and Mackenzie, 1990; Luo and Vasseur, 1996).

In the following analysis, I compute the variations in pore and fluid volume, which allow the calculation of the rock porosity and saturations as a function of pore pressure, the independent variable. These variations take place at nearly constant confining pressure (i.e., constant depth) and temperature. The changes are solely due to compressibility effects, since at nearly constant temperature thermal effects can be neglected. The reference state, for which all the properties are known, is the hydrostatic state. I consider constant composition within each phase, since the aim is to study variations due to pure pressure effects rather than changes due to variations in material composition. Thus, the model does not apply to mechanisms of overpressure generation such as shale dehydration and kerogen maturation. A pressure model for variable composition is given by Berg and Gangi (1999), who calculate the excess pore pressure as a function of the fraction of kerogen converted to oil and the fraction of oil converted to gas. This model can easily be incorporated in the present theory.

I assume a closed rock unit at a fixed depth z and temperature T. Here, a pressure compartment, which is characterized by an effective seal that prevents pressure equilibration to normal hydrostatic pressure (Bradley and Powley, 1994). The lithostatic pressure for an average sediment density $\bar{\rho}$ is equal to $p_c = \bar{\rho} g z$, where g is the acceleration due to gravity. On the other hand, the normal hydrostatic pore pressure is approximately $p_H = \rho_w g z$, where ρ_w is the density of brine.

In general, seismic properties, such as wave velocity and attenuation, depend on effective pressure:

$$p_e = p_c - np, \tag{1}$$

where p_e, p_c, and p are the effective, confining, and pore pressures, respectively, and $n \leq 1$ is the effective stress coefficient. Note that the effective pressure equals the confining pressure at zero pore pressure. It is found that $n \approx 1$ for static measurements of the compressibilities (Zimmerman et al., 1986). In dynamic experiments, n is approximately linearly dependent on the differential pressure $p_d = p_c - p$ (Gangi and Carlson, 1996; Prasad and Manghnani, 1997): $n = n_0 - n_1 p_d$, where n_0 and n_1 are constant coefficients. Using this equation, the effective pressure (1) can be written as

$$p_e = p_c - (n_0 - n_1 p_c)p - n_1 p^2. \tag{2}$$

I know the porosity and fluid saturations at the hydrostatic pressure, and I want to compute these quantities at a pore pressure higher than the hydrostatic. Assuming oil, gas, and brine in the pore space, the volume balance is

$$V_{\text{pore}} = V_o + V_g + V_w, \tag{3}$$

where V_{pore} is the pore volume, and V_o, V_g, and V_w are the volumes of oil, gas, and brine in the pore space, respectively. Since no mass (of the organics or the brine) leave the pore space, and the depth remains constant, the volume changes do not depend on mass and temperature. The pore-space and oil, gas, and brine compressibilities are defined as

$$c_p = -\frac{1}{V_{\text{pore}}}\frac{dV_{\text{pore}}}{dp_e}, \quad c_o = -\frac{1}{V_o}\frac{dV_o}{dp},$$
$$c_g = -\frac{1}{V_g}\frac{dV_g}{dp}, \quad c_w = -\frac{1}{V_w}\frac{dV_w}{dp}, \tag{4}$$

respectively. Note that the pore "senses" the effective pressure, but the fluid "sense" the pore pressure.

I assume that the compressibilities of the oil and brine are independent of pressure, and those of the gas and the rock depend on pressure. Moreover, I consider the following functional form for c_p as a function of effective pressure:

$$c_p = c_p^{\infty} + \alpha p_e + \beta \exp\left(-p_e/p^*\right), \tag{5}$$

where c_p^{∞}, α, β, and p^* are coefficients obtained by fitting the experimental data. Similar functional forms (5) are used to fit experimental data of pore compressibility (Zimmerman et al., 1986; Prasad and Manghnani, 1997).

Integration of equations (4) from the hydrostatic pressure $p_i = p_H$ to a given pore pressure p yields

$$V_{\text{pore}}(p) = V_{\text{pore}\,i} \exp[E(\Delta p)], \tag{6}$$

$$V_o(p) = V_{oi} \exp(-c_o \Delta p), \tag{7}$$

$$V_g(p) = V_{gi} \exp\left(-c_g \int_{p_i}^{p} c_g(p)\, dp\right), \tag{8}$$

and

$$V_w(p) = V_{wi} \exp(-c_w \Delta p), \tag{9}$$

where $\Delta p = p - p_H$,

$$E(\Delta p) = -c_p^{\infty}\Delta p_e + \frac{1}{2}\alpha\left(p_e^2 - p_{ei}^2\right) + \beta p^*\left[\exp\left(-p_e/p^*\right) - \exp\left(-p_{ei}/p^*\right)\right],$$

and $\Delta p_e = p_e - p_{ei}$. Index i denotes the initial (hydrostatic) state, and p_{ei} is the effective pressure at the initial state.

Using equations (6) and (7)–(9), and since the initial saturations for brine, oil, and gas, respectively, are

$$S_{wi} = V_{wi}/V_{\text{pore}\,i}, \quad S_{oi} = V_{oi}/V_{\text{pore}\,i}, \quad S_{gi} = V_{gi}/V_{\text{pore}\,i}, \tag{10}$$

the pore-volume balance equation (3) becomes

$$\exp[E(\Delta p)] = S_{wi}\exp(-c_w\Delta p) + S_{oi}\exp(-c_o\Delta p) + S_{gi}\exp\left(-c_g\int_{p_i}^{p} c_g(p)\,dp\right). \tag{11}$$

As the pore pressure changes from p_i to p, the pore volume changes from $V_{\text{pore}\,i}$ to $V_{\text{pore}\,i}\exp[E(\Delta p)]$. The saturations are equal to the corresponding volumes divided by the pore volume. Using equations (7) and (9), the requirement that $S_{gi} = 1 - S_{wi} - S_{oi}$, gives for the oil, brine, and gas saturations

$$S_o = S_{oi}\exp[-c_o\Delta p - E(\Delta p)] \tag{12}$$

$$S_w = S_{wi}\exp[-c_w\Delta p - E(\Delta p)], \tag{13}$$

and

$$S_g = 1 - S_w - S_o, \tag{14}$$

respectively. On the other hand, the fluid proportions for oil, brine, and gas, respectively, are

$$\phi_o = \phi S_o, \quad \phi_w = \phi S_w, \quad \phi_g = \phi S_g, \tag{15}$$

where $\phi = V_{\text{pore}}/(V_{\text{pore}} + V_s)$ is the total porosity, with V_s the volume of the solid part. This can be calculated from the initial porosity ϕ_i (at hydrostatic pressure), since $\phi_i = V_{\text{pore}\,i}/(V_{\text{pore}\,i} + V_s)$. Thus, since $V_s = V_{\text{pore}\,i}(1/\phi_i - 1)$ and using (6), I obtain

$$\phi = \frac{\phi_i\exp[E(\Delta p)]}{1 - \phi_i\{1 - \exp[E(\Delta p)]\}}, \tag{16}$$

assuming incompressible grains in this calculation ($V_s \approx$ constant). Defining ϕ_s as the mineral matrix fraction, $\phi_s = 1 - \phi$. The pressure model can be refined by assuming the dependence on pressure and temperature of oil and brine compressibilities, and the influence of sodium chloride on brine properties. If one considers, for instance, the empirical formulas published by Batzle and Wang (1992), the solution can be obtained by numerical integration of the compressibilities.

Compressibilities and dry-rock bulk moduli

The isothermal gas bulk modulus K_g and the gas compressibility $c_g = K_g^{-1}$ depend on pressure. The latter can be calculated from the van der Waals equation:

$$\left(p + a\rho_g^2\right)(1 - b\rho_g) = \rho_g RT, \tag{17}$$

where p is the gas pressure, ρ_g is the gas density, T is the absolute temperature, and R is the gas constant. Moreover, a good approximation can be obtained using $a = 0.225$ Pa $(\text{m}^3/\text{mole})^2 = 879.9$ MPa $(\text{cm}^3/\text{g})^2$ and $b = 4.28\times10^{-5}$ $\text{m}^3/\text{mole} = 2.675$ cm^3/g (one mole of methane, CH_4, corresponds to 16 g). Then,

$$c_g = \frac{1}{\rho_g}\frac{d\rho_g}{dp} = \left[\frac{\rho_g RT}{(1 - b\rho_g)^2} - 2a\rho_g^2\right]^{-1}. \tag{18}$$

In sandstones, the pore compressibility c_p is closely related to the bulk modulus of the matrix K_m [the compressibility c_p is denoted by C_{pp} in Zimmerman et al. (1986) and by $K_{\phi p}^{-1}$ in Mavko and Mukerji (1995), and K_m corresponds to C_{bc}^{-1} and K_{dry}^{-1}, respectively]. Using the present notation, c_p can approximately be expressed as

$$c_p = \left(\frac{1}{K_m} - \frac{1}{K_s}\right)\frac{1}{\phi} - \frac{1}{K_s}, \tag{19}$$

where ϕ depends on the pore pressure difference Δp at constant confining pressure. Since dry-rock wave velocities are practically frequency independent, the seismic moduli K_m and μ_m versus confining pressure can be obtained from laboratory measurements in dry samples. If V_{P0} and V_{S0} are the experimental dry-rock compressional and shear velocities, the moduli are given approximately by

$$K_m = (1 - \phi)\rho_s\left(V_{P0}^2 - \frac{4}{3}V_{S0}^2\right), \quad \mu_m = (1 - \phi)\rho_s V_{S0}^2, \tag{20}$$

where ρ_s is the grain density and ϕ is the porosity. I recall that K_m is the rock modulus at almost zero pore pressure, i.e., the case when the bulk modulus of the pore fluid is negligible compared with the frame bulk modulus, as for example air at room conditions (Mavko and Mukerji, 1995).

SEISMIC PROPERTIES OF THE ROCK-VOLUME AND REFLECTION COEFFICIENTS OF THE SEAL

The seismic velocities of the overpressured porous rock are computed by using Biot's theory of dynamic poroelasticity (Biot, 1962; Carcione, 1998). Fluid saturations and porosity versus pore pressure are given by equations (12), (13), (14), and (16). Other properties involved in the theory are given in Table 1: grain, oil, gas, and water densities and bulk moduli, ρ_s, ρ_o, ρ_g, and ρ_w, and K_s, K_o, K_g, and K_w, respectively; grain shear modulus, μ_s; oil, gas, and water viscosities, η_o, η_g and η_w, respectively; permeability, κ; tortuosity, T; and dry-rock moduli, K_m and μ_m.

The mixture of organics and brine behaves as a composite fluid with properties depending on the constants of the constituents and their relative concentrations. This problem has been analyzed by Berryman et al., (1988). The mixture density and viscosity are the arithmetic average of the fluid densities and viscosities weighted by the respective saturations. On the other hand, the mixture bulk modulus is computed by using Wood's model (Berryman et al., 1988).

A multiple seal consists of interbedded shale and sandstone units. The calculation of the reflection coefficient of the seal is developed in Appendix B, where sandstone is isotropic and shale is transversely isotropic. For an incident compressional wave (subscript P), the reflection and transmission coefficient vector $\mathbf{r} = [R_{PP}, R_{PS}, T_{PP}, T_{PS}]^\top$ is

$$\mathbf{r} = -(\mathbf{A}_1 - \mathbf{B}\mathbf{A}_2)^{-1}\mathbf{i}_P, \tag{21}$$

where $\mathbf{A}_1$ and $\mathbf{A}_2$ are the propagator matrices related to the upper and lower media [equations (A-24) and (A-26), respectively], $\mathbf{B}$ is the propagator matrix of the seal [(A-9)], and $\mathbf{i}_P$ is the incidence vector [(A-23)]. The two isotropic half-spaces above and below the seal, and the interbedded sandstone units correspond to the abnormally pressured rock. As already mentioned, their phase velocities and densities are calculated by using Biot's theory and are directly introduced in the reflection-transmission equations. No attempt is made to calculate explicitly the reflection coefficient of single-phase layers (shales) embedded in a two-phase medium (the rock volume).

EXAMPLES

I assume a sandstone at $z = 3$ km depth. If the average sediment density is $\bar{\rho} = 2.4$ g/cm^3, the confining pressure is $p_c = 70.6$ MPa and the hydrostatic pressure $p_H = 30.6$ MPa (assuming $\rho_w = 1.04$ g/cm^3). For a constant geothermal gradient, G, the temperature of a particular sediment volume is $T = T_0 + Gz$, where T_0 is the temperature at the surface. With a surface temperature of 25°C and a gradient $G = 25$ °C/km, $T = 100$°C.

Experimental data of wave velocities versus pore and confining pressure are available in Table 1 of Christensen and Wang (1985), where I assume that the experiments at zero pore pressure yield the properties of the dry rock. This is not strictly true at ultrasonic frequencies, since the fluid is in an unrelaxed state, but it constitutes a reasonable approximation when dry-rock velocity measurements are not available. On the basis of equations (20), following the form of equation (5) and Christensen and Wang's (1985) data for p_c ranging from 0 to 70 MPa, best-fit estimates of the dry-rock moduli versus confining pressure are

$$K_m[\text{GPa}] = 21.29 + 0.015\,p_c[\text{MPa}] - 5.5\exp(-p_c[\text{MPa}]/12.49),$$

Table 1. Material properties for Berea sandstone at 3 km depth and hydrostatic pore pressure.

Property	Value
Grain	
ρ_s	2650 kg/m^3
K_s	37 GPa
μ_s	39 GPa
Fluids	
ρ_o	700 kg/m^3
K_o	0.57 GPa
η_o	68 cP
ρ_g	111 kg/m^3
K_g	0.043 Pa
η_g	0.013 cP*
ρ_w	1040 kg/m^3
K_w	2.25 GPa
η_w	1.8 cP*
Matrix	
K_m	21.73 GPa
μ_m	12.21 GPa
ϕ	0.2
κ	10^{-12} m^2
T	2

*1 cP = 0.001 Pa · s.

and

$$\mu_m[\text{GPa}] = 11.35 + 0.02\,p_c[\text{MPa}] - 6.1\exp(-p_c[\text{MPa}]/5.68),$$

and c_p in MPa is given by equation (5), with $c_p^\infty = 0.075$ GPa^{-1}, $\alpha = -0.00019$ (MPa GPa)$^{-1}$, $\beta = 0.08$ GPa^{-1}, $p^* = 9.87$ MPa, and the pressure given in MPa. The pore compressibility c_p has been obtained from equation (19) by assuming that the porosity is that at hydrostatic pore pressure [this approximation is supported by experimental data obtained by Domenico (1977) and Han et al. (1986)]. The best-fit plots for K_m and μ_m (a) and c_p (b) versus pore pressure are illustrated in Figure 1.

In order to obtain the moduli for different combinations of the confining and pore pressures, we should make the substitution $p_c \to p_e = p_c - np$, where I assume, following Gangi and Carlson (1996), that n depends on differential pressure as $n = n_0 - n_1 p_d$. This dependence of n versus differential pressure is in good agreement with the experimental values corresponding to the compressional velocity obtained by Christensen and Wang (1985) and Prasad and Manghnani (1997). Experimental evidence indicates that n is different for each physical property.

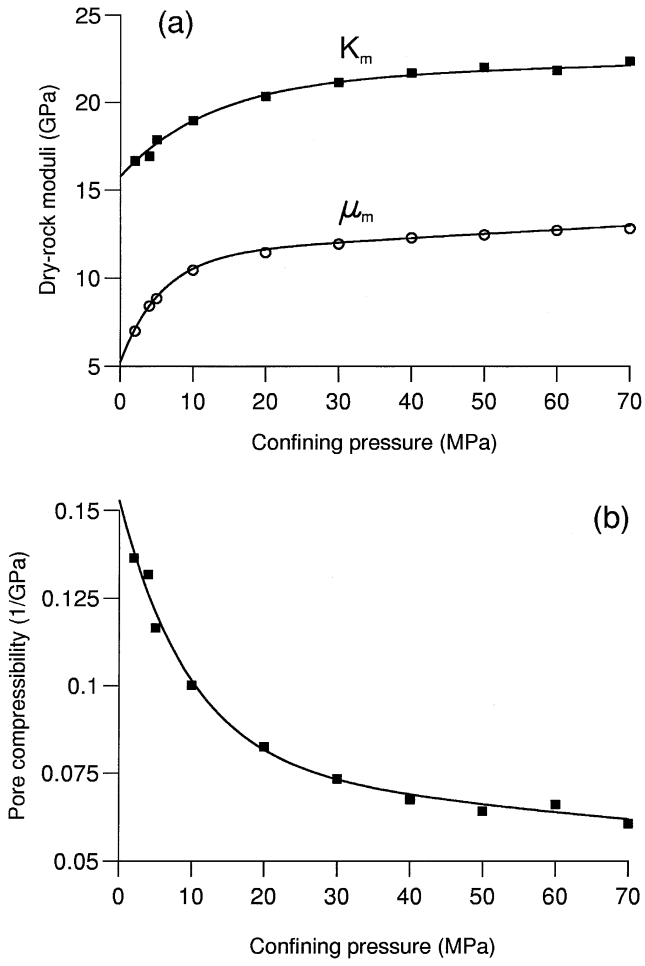

FIG. 1. Regression fits to dry-rock moduli K_m and μ_m (a) and pore compressibility c_p (b) obtained from the experimental data for Berea sandstone published by Christensen and Wang (1985).

A linear best fit of the values provided by Christensen and Wang (1985) yield

$$\text{bulk modulus and compressibility:} \quad n_0 = 0.886,$$
$$n_1 = 0.0039\ \text{MPa}^{-1}$$

and

$$\text{shear modulus:} \quad n_0 = 1.015, \quad n_1 = 0.0014\ \text{MPa}^{-1},$$

with the moduli given in GPa and the compressibility in GPa^{-1}. Table 1 indicates the properties for Berea sandstone, where the values correspond to those at the initial (hydrostatic) pore pressure. The oil and brine densities and bulk moduli are assumed pressure independent; the oil and gas viscosities as a function of pore pressure are taken from Luo and Vasseur (1996). The continuous line in Figure 2 shows the compressional velocity versus pore pressure for a constant confining pressure $p_c = 70.6$ MPa. Christensen and Wang (1985) provide the experimental velocities for full brine saturation ($S_{wi} = 1$) and different pore and confining pressures. Knowing n, it is possible to obtain the velocities for different combinations of the pore and confining pressures, in particular for $p_c = 70.6$ MPa and variable pore pressure. Each experimental point in Figure 2 (from Table 1 of Christensen and Wang, 1985) corresponds to a pore pressure p that is a solution of the second-degree equation (2). The n values corresponding to the compressional velocity given in Table 2 of Christensen and Wang (1985) are used to obtain the effective pressure. The velocity decreases substantially with increasing pore pressure, probably due to the opening of compliant cracks. This information is contained in the behavior of the dry-rock moduli as a function of confining pressure. The experimental points between 40 and 50 MPa correspond to confining pressures higher than 100 MPa. The discrepancy with the theoretical curve is due to the fact that the dry-rock moduli were computed with data at confining pressure less than 70 MPa.

In the following, I assume an initial gas saturation $S_{gi} = 0.8$ and brine saturation $S_{wi} = 0.05$, which are reasonable values at the top of a reservoir. Figure 3 shows the calculated wave velocities versus pore pressure at a confining pressure of 70.6 MPa. Note that the P-wave velocity is higher than the P-wave velocity for full water saturation (see Figure 2), since the decrease in density dominates over the decrease in bulk modulus of the fluid mixture for the rock under these conditions.

Shale layers are modeled as a transversely-isotropic high-velocity, high-density medium (Johnston and Christensen, 1995), with properties $c_{11} = 60$ MPa, $c_{33} = 50$ MPa, $c_{13} = 16$ MPa, $c_{55} = 16$ MPa, and $\rho = 2700$ kg/m^3 (the low stiffnesses for shale take into account a fluid softening effect by hydration). These properties are assumed to be independent of pressure. In principle, variations of wave velocities with pore pressure are less than those observed for sandstones of similar porosity (Johnston, 1987).

The central frequency of the seismic pulse is assumed to be $f_0 = 25$ Hz. Then, the average wavelengths of the signal corresponding to the upper formation are 168 m for P-waves and

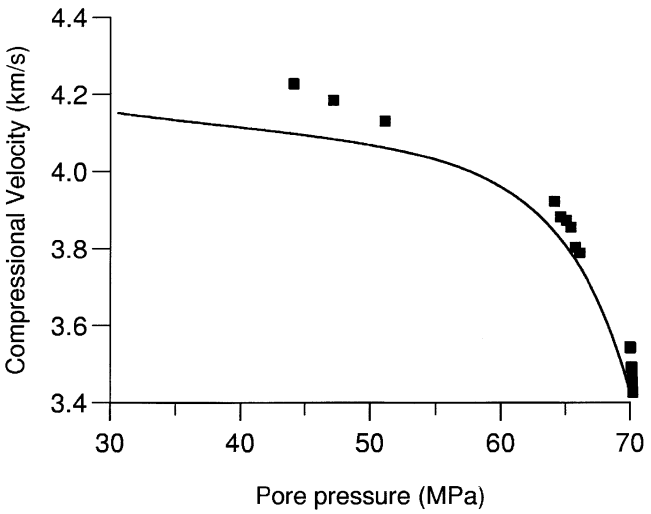

FIG. 2. Compressional velocity as a function of pore pressure for a confining pressure of 70.6 MPa and full water saturation. The experimental points are from Table 1 Christensen and Wang (1985).

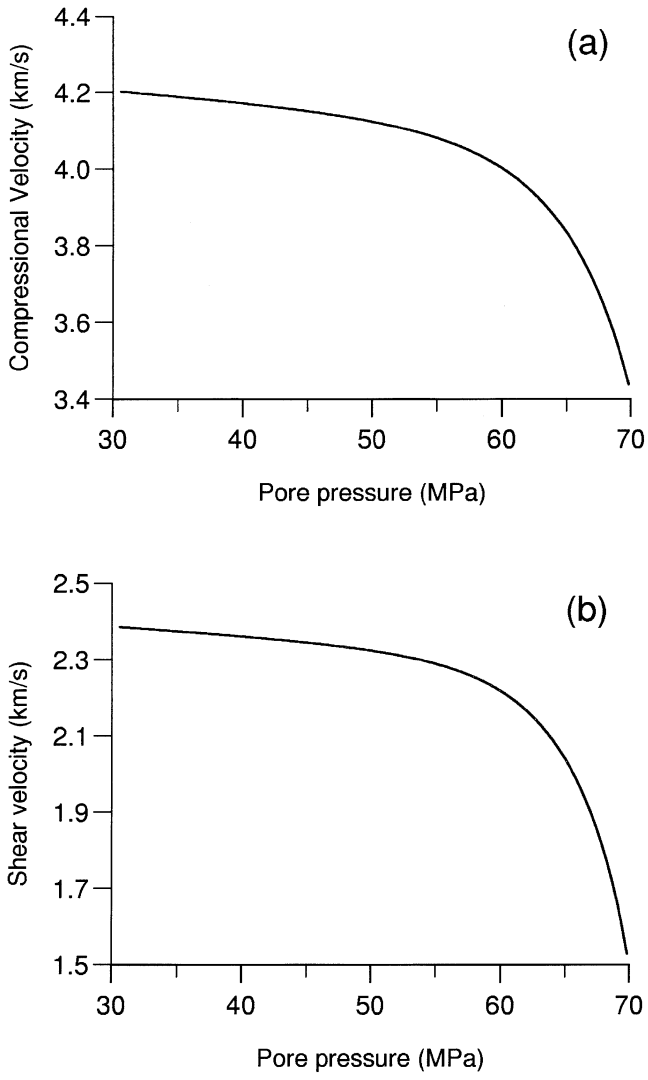

FIG. 3. Calculated compressional (a) and shear velocities (b) as a function of pore pressure for a confining pressure of 70.6 MPa. The initial gas saturation is $S_{gi} = 0.8$ and the initial brine saturation is $S_{wi} = 0.05$.

95 m for S-waves. I consider that the seal thickness is much smaller than the wavelength of the P-wave seismic pulse. Seal thicknesses smaller than the seismic wavelength were reported by Bradley (1985) at shallow depths and Powley in exploration wells (Bradley and Powley, 1994), with a thickness of approximately 90 m at 5200 m depth (see also Deming, 1994). In the following analysis, we refer to a positive (negative) AVO trend or anomaly when the absolute value of the reflection coefficient increases (decreases).

Single shale layer

I assume that the upper medium is at hydrostatic pressure, and the lower medium at a pore pressure higher than the hydrostatic. The seal is a shale layer with the properties indicated above (see Figure A-1). Figure 4 shows the absolute values of the amplitude reflection coefficients R_{PP} (continuous lines) and R_{PS} (broken lines) for seal thicknesses $h=0$ (a) and $h=80$ m (b). As expected, strong AVO effects are associated with high pore pressures approaching the confining pressure. The P-wave anomaly is negative for $h=0$, and changes from negative to positive when the thickness of the seal is 80 m (half the P-wave wavelength). Moreover, S-wave AVO anomalies, in general, are stronger than P-wave anomalies for incidence angles less than 40°.

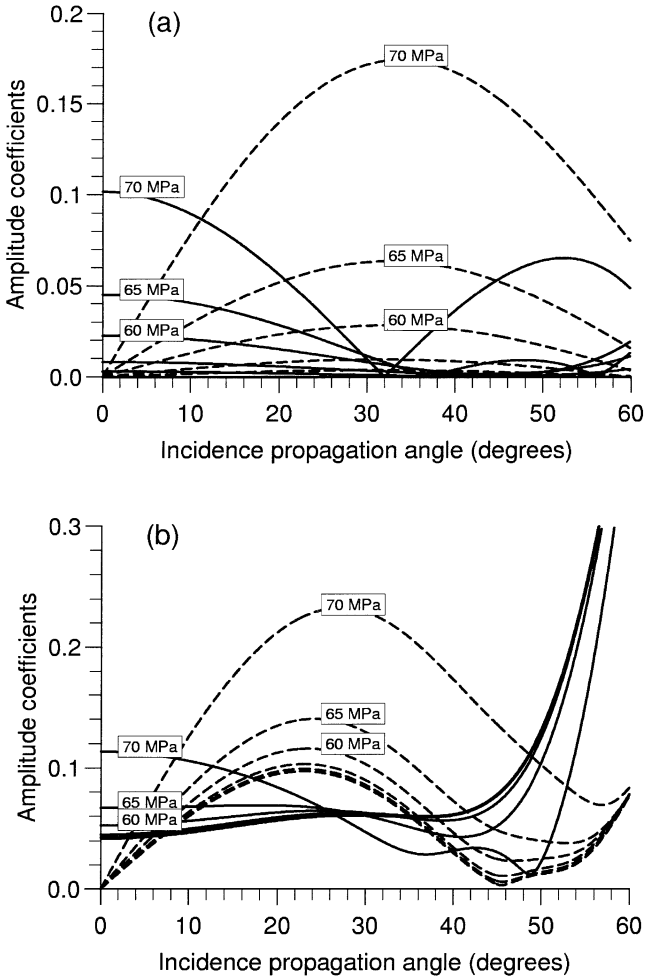

FIG. 4. Absolute values of the amplitude reflection coefficients R_{PP} (continuous lines) and R_{PS} (broken lines) for calculated rock properties at 3 km depth for seal thicknesses $h=0$ (a) and $h=80$ m (b). The upper medium is at hydrostatic pore pressure (30 MPa). The pore pressure of the lower medium ranges from 30 to 70 MPa; some values are indicated in the figure. The lower curves at normal incidence correspond to the hydrostatic pressure (30.6 MPa).

Pressure transition in sandstone

In this case, the seal is a transition zone with a high-pressure gradient (Figure 5). The properties of the seal are obtained by assuming $N=50$ thin layers (thin compared with the seismic wavelengths) of thickness h/N. Figure 6 shows absolute values of the amplitude reflection coefficients R_{PP} (continuous lines) and R_{PS} (broken lines) at 3 km depth for a seal thickness $h=80$ m. The situation is similar to case (a) of the previous example ($h=0$). The P-wave anomaly is negative and the S-wave anomaly is positive for exploration incidence angles (say, less than 40°).

Interbedded shale and sandstone units

This example considers a series of parallel thin layers of interbedded shale and sandstone that are increasingly effective (in terms of sealing efficiency) with depth. This situation is illustrated in Figure 7, where shale layers are embedded in the rock volume to constitute a multiple seal (see the real-data example in Figure 12 of Bradley and Powley, 1994). This situation also occurs at fault surfaces by shale smearing in mixed sandstone/shale formations (Sassi et al., 1992). The seal is divided into 25 sandstone/shale layers of thickness $h/25$, with pore pressure increasing linearly with depth. Shale proportion equals sandstone proportion. Figure 8 shows absolute values

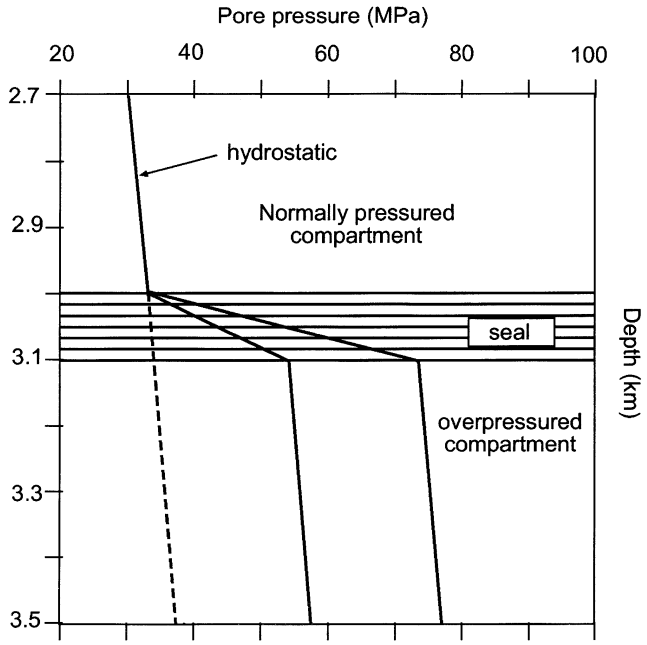

FIG. 5. Pore pressure transition seal in sandstone. The seal is a set of thin sandstone layers at different pore pressures, increasing linearly with depth.

of the amplitude reflection coefficients R_{PP} (continuous lines) and R_{PS} (broken lines) for seal thickness $h = 40$ and $h = 80$ m, respectively.

Figure 9 shows the *PP*-reflection coefficients versus seal thickness for an incidence angle of 10°, and pore pressures ranging from 30 to 70 MPa. Interference effects result in an oscillatory behavior with thickness. The oscillatory character of the curves implies an ambiguity of the coefficients with respect to the layer thickness because two or more values of h may correspond to the same value of the reflection coefficient. The period of the oscillations depends on the frequency, the layer thickness, and the wave velocity, according to the exponentials functions in equation (A-26). For instance, minimum values of the *PP*-reflection coefficients are obtained by setting $(\omega_0/V_P)h = \pi$, where $\omega_0 = 2\pi f_0$ and V_P is the average phase velocity of the *P*-wave in the seal along the refracted ray. For increasing (decreasing) frequencies, the period of the oscillations decreases (increases). In practice, however, this ambiguity can be solved, since for a layer thickness greater than, say, $\pi V_{ph}/(2\omega_0)$, the top and bottom seismic events can be distinguished.

Finally, we obtain the AVO intercept, A, and the AVO gradient, B, for each case, based on Shuey's two-term approximation $R(\theta) = A + B\sin^2(\theta)$, where R is the *PP*-reflection coefficient and θ is the angle of incidence (Castagna and Swan, 1997). Figures 10a and 10b show the A/B crossplots, corresponding to the last example (Figures 8a and 8b). The anomalies are class I and class IV, respectively. The crossplots for the first and second examples can be shown to be class IV.

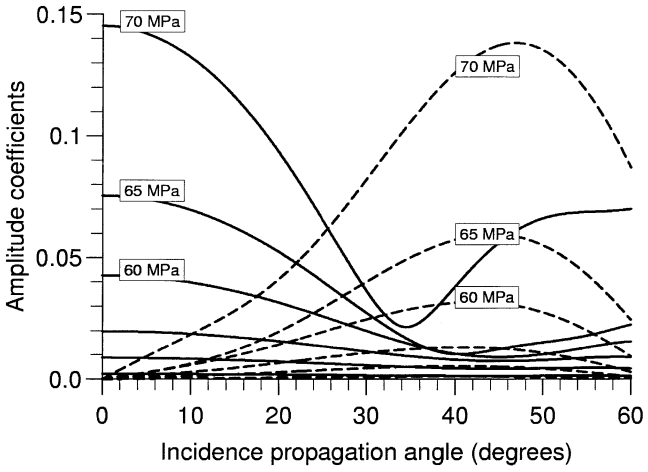

FIG. 6. Absolute values of the amplitude reflection coefficients R_{PP} (continuous lines) and R_{PS} (broken lines) at 3 km depth. The seal, of 80 m thickness, is a pressure transition zone in sandstone. The upper medium is at hydrostatic pore pressure (30 MPa). The pore pressure of the lower medium ranges from 30 to 70 MPa; some values are indicated in the figure. The lower curves at normal incidence correspond to the hydrostatic pressure (30.6 MPa).

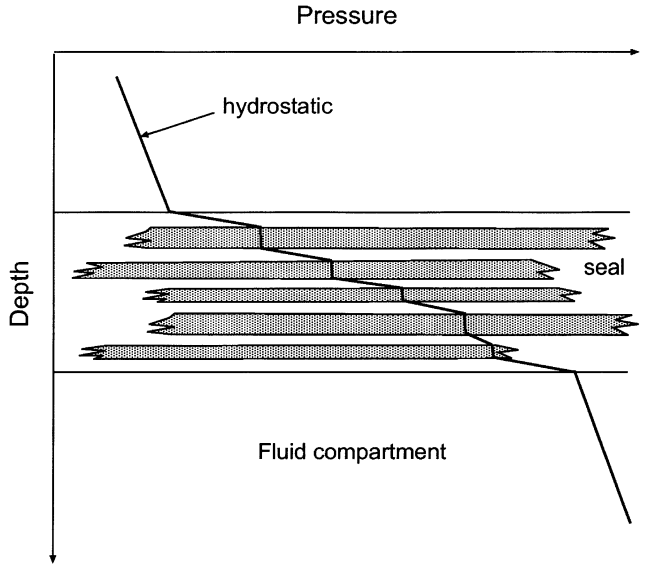

FIG. 7. Pressure seal formed by thin sandstone and shale layers. The pore pressure increases linearly with depth inside the seal.

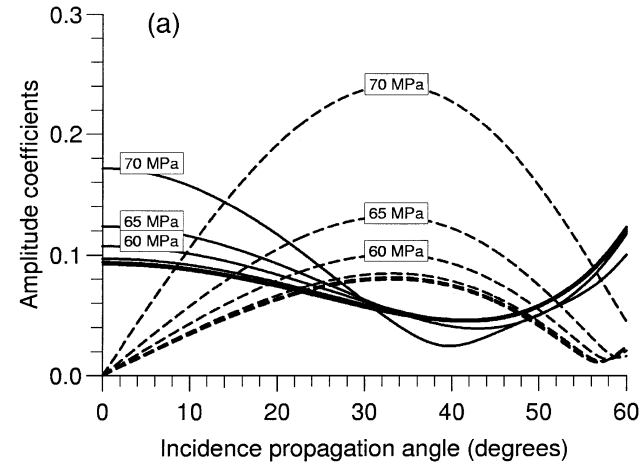

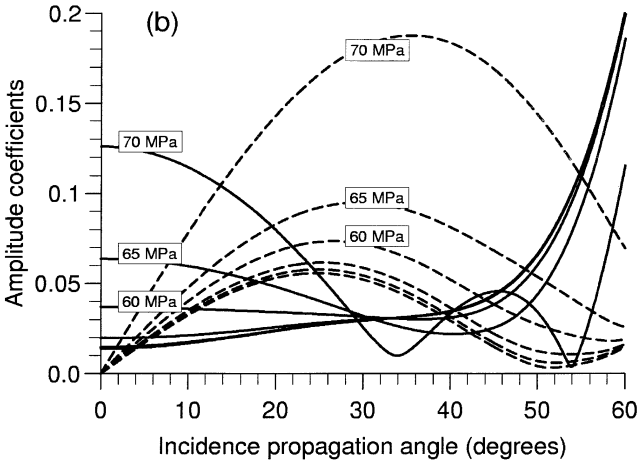

FIG. 8. Absolute values of the amplitude reflection coefficients R_{PP} (continuous lines) and R_{PS} (broken lines) at 3 km depth for seal thicknesses $h = 40$ (a) and $h = 80$ m (b). The seal is a set of interbedded shale and sandstone thin layers, with equal composition. The upper medium is at hydrostatic pore pressure (30 MPa). The pore pressure of the lower medium ranges from 30 to 70 MPa; some values are indicated in the figure. The lower curves at normal incidence correspond to the hydrostatic pressure (30.6 MPa).

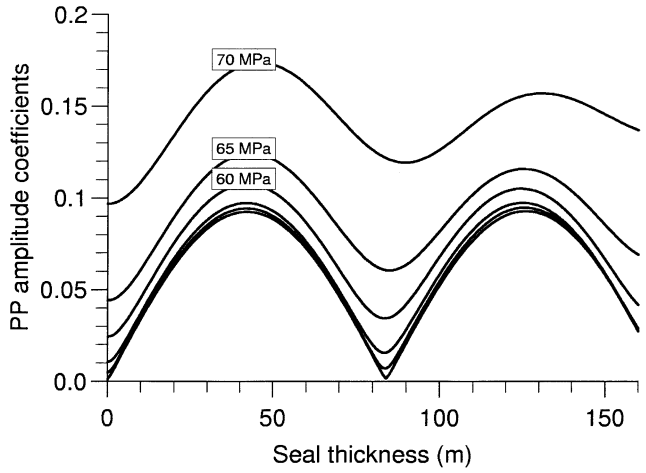

FIG. 9. *PP*-reflection coefficients versus seal thickness for an incidence angle of 10° and pore pressures ranging from 30 to 70 MPa. The seal is a set of interbedded shale and sandstone thin layers, with equal composition, as in Figures 7 and 8. The lower curve at normal incidence corresponds to the hydrostatic pressure (30.6 MPa).

CONCLUSIONS

This study shows the expected influence of abnormal pore pressures on AVO information. The model relating pore pressure to seismic velocity requires calibration with laboratory measurements of wave velocities versus confining and pore pressures. I assume that zero pore pressure measurements give the dry-rock moduli and pore compressibility, which include microstructural information, such as the effects of closing of compliant cracks. In addition, experiments on saturated samples for different confining and pore pressures give the effective stress coefficient n, which allows the calculation of the seismic property versus effective pressure.

The seismic velocities of the overpressured rock, saturated with gas, oil, and brine, are obtained by Biot's theory. The AVO behavior is obtained by computing the reflection coefficients of a set of thin sandstone/shale layers embedded between two sandstone at different pore pressures.

Strong and negative AVO effects are associated with high pore pressures, approaching the confining pressure. For negligible seal thickness or shale-free transitions, the *PP* AVO anomaly is negative at near and moderate offsets. For Berea sandstone and a shaly seal, the *PP* anomaly is negative for negligible seal thicknesses, and can be positive or negative, depending on pore pressure, when the seal thickness approaches half the wavelength of the seismic signal. *PS* anomalies, in general, are positive and stronger than *PP* anomalies for exploration incidence angles (say, less than 40°). The reflection coefficients versus seal thickness have an oscillatory character, with the period of the oscillations depending on the frequency of the signal and the wave velocities of the seal.

ACKNOWLEDGMENTS

This work was supported by Norsk Hydro a.s. (Bergen), and by the European Union under the project "Detection of overpressure zones with seismic and well data." Thanks to Michael Batzle for a detailed review and Fabio Cavallini and Hans Helle for important technical comments.

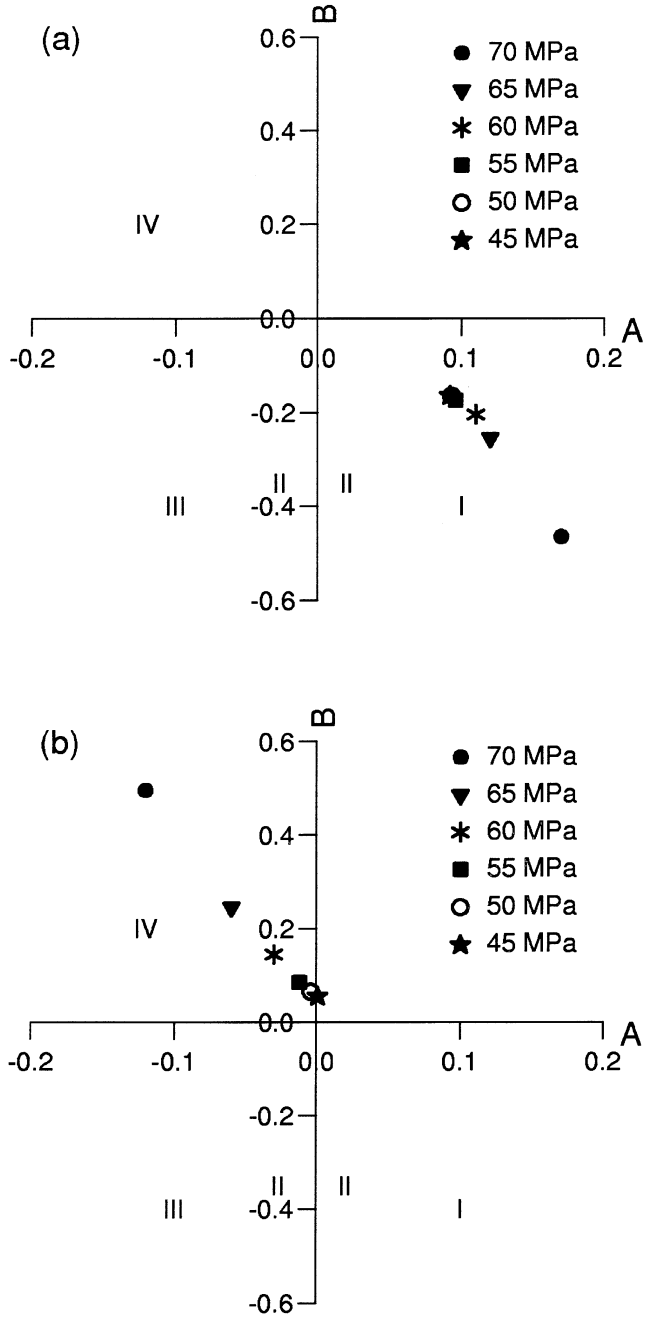

FIG. 10. *PP* AVO crossplots corresponding to the example illustrated in Figure 8.

REFERENCES

Batzle, M., and Wang, Z., 1992, Seismic properties of pore fluids: Geophysics, **57**, 1396–1408.
Benzing, W. M., and Shook, G. M., 1996, Study advances view of geopressure seals: Oil & Gas J., May, 62–66.
Berg, R. R., and Gangi, A. F., 1999, Primary migration by oil-generation microfracturing in low-permeability source rocks: Application to the Austin chalk, Texas: AAPG Bull., **83**, 727–756.
Berryman, J. G., Thigpen, L., and Chin, R. C. Y., 1988, Bulk elastic wave propagation in partially saturated porous solids: J. Acous. Soc. Am., **84**, 360–373.
Bilgeri, D., and Ademeno, E. B., 1982, Predicting abnormally pressured sedimentary rocks: Geophys. Prosp., **30**, 608–621.
Biot, M. A., 1962, Mechanics of deformation and acoustic propagation in porous media: J. Appl. Phys., **33**, 1482–1498.

Bradley, J. S., 1985, Safe disposal of toxic and radioactive liquid wastes: Geology, **13**, 328–329.
Bradley, J. S., and Powley, D. E., 1994, Pressure compartments in sedimentary basins: A review, *in* Ortoleva, J., Ed., Basin compartments and seals: Am. Assn. Petr. Geol. Memoir **61**, 3–26.
Brekhovskikh, L. M., 1960, Waves in layered media: Academic Press.
Carcione, J. M., 1997, Reflection and transmission of *qP*-*qS* plane waves at a plane boundary between viscoelastic transversely isotropic media: Geophys. J. Internat., **129**, 669–680.
——— 1998, Viscoelastic effective rheologies for modeling wave propagation in porous media, Geophys. Prosp., **46**, 249–270.
Castagna, J. P., and Swan, H. W., 1997, Principles of AVO crossplotting: The Leading Edge, 337–342.
Chiarelli, A., and Duffaud, F., 1980, Pressure origin and distribution in Jurassic of Viking basin (United Kingdom–Norway): AAPG Bull., **64**, 1245–1266.
Christensen, N. I., and Wang, H. F., 1985, The influence of pore pressure and confining pressure on dynamic elastic properties of Berea sandstone: Geophysics, **50**, 207–213.
Deming, D., 1994, Factors necessary to define a pressure seal: AAPG Bull., **78**, 1005–1009.
Domenico, S. N., 1977, Elastic properties of unconsolidated porous sand reservoirs: Geophysics, **42**, 1339–1368.
Gangi, A. F., and Carlson, R. L., 1996, An asperity-deformation model for effective pressure: Tectonophysics, **256**, 241–251.
Han, D., Nur, A., and Morgan, D., 1986, Effects of porosity and clay content on wave velocities in sandstones: Geophysics, **51**, 2093–2107.
Heath, A. E., Walsh, J. J., and Watterson, J., 1994, Estimation of the effects of sub-seismic sealing faults on effective permeabilities in sandstone reservoirs: North Sea Oil and Gas Reservoirs, III, 173–183.
Iverson, W. P., Martinsen, R. S., and Surdam, R. C., 1994, Pressure seal permeability and two-phase flow, *in* Ortoleva, J., Ed., Basin compartments and seals: Am. Assn. Petr. Geol. Memoir **61**, 313–319.
Johnston, D. H., 1987, Physical properties of shale at temperature and pressure: Geophysics, **52**, 1391–1401.
Johnston, J. E., and Christensen, N. I., 1995, Seismic anisotropy of shales: J. Geophys. Res., **100**, 5991–6003.
Law, B. E., Ulmishek, G. F., and Slavin, V. I., Eds., 1998, Abnormal pressures in hydrocarbon environments: Am. Assn. Petr. Geol. Memoir **70**.
Louis, J. N., and Asad, A. M., 1994, Seismic amplitude versus offset (AVO) character of geopressured transition zones, *in* Ortoleva, J., Ed., Basin compartments and seals: Am. Assn. Petr. Geol. Memoir **61**, 131–137.
Luo, X., and Vasseur, G., 1996, Geopressuring mechanism of organic matter cracking: numerical modeling: AAPG Bull., **80**, 856–874.
Mann, D. M., and Mackenzie, A. S., 1990, Prediction of pore fluid pressures in sedimentary basins, Marine and Petr. Geol., **7**, 55–65.
Mavko, G., and Mukerji, T., 1995, Seismic pore space compressibility and Gassmann's relation: Geophysics, **60**, 1743–1749.
Prasad, M., and Manghnani, M. H., 1997, Effects of pore and differential pressure on compressional wave velocity and quality factor in Berea and Michigan sandstones: Geophysics, **62**, 1163–1176.
Sassi, W., Livera, S. E., and Caline, B. P. R., 1992, Reservoir compartmentation by faults in Cormorant Block IV, U.K. northern North Sea, *in* Larsen, R. M., Ed., Structural and tectonic modelling and its application to petroleum geology: Norwegian Petr. Soc., Special Publication **1**, 355–364.
Thomson, W. T., 1950, Transmission of elastic waves through a stratified solid material: J. Appl. Phys., **21**, 89.
Zimmerman, R. W., Somerton, W. H., and King, M. S., 1986, Compressibility of porous rocks: J. Geophys. Res., **91**, 12765–12777.

APPENDIX A

REFLECTION COEFFICIENTS OF A SET OF TRANSVERSELY ISOTROPIC LAYERS EMBEDDED BETWEEN TWO ISOTROPIC HALF-SPACES

Assume a transversely-isotropic layer whose elastic constants are denoted by c_{IJ}, $I, J = 1, \ldots, 6$. A plane wave with horizontal complex slowness s incides on the symmetry plane of the layer from above, as shown in Figure A-1. Inside the layer, the particle velocity field is a superposition of upgoing and downgoing quasi-compressional (P) and quasi-shear waves (S) of the form

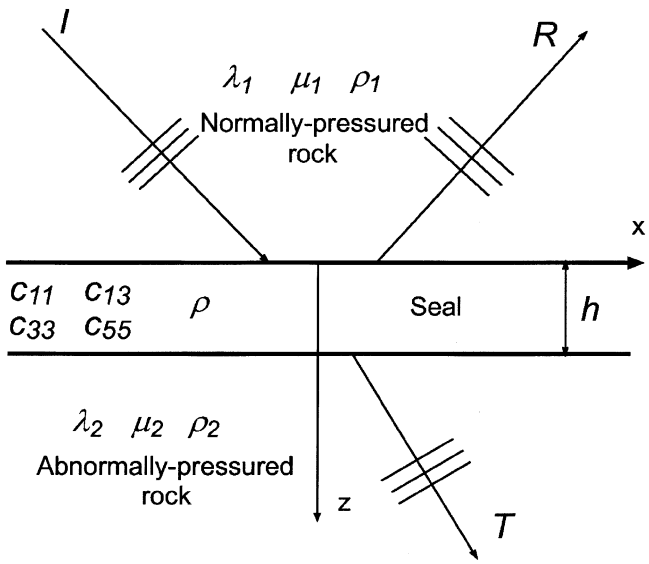

FIG. A-1. Diagram showing a transversely-isotropic layer (seal) embedded between two isotropic media (sandstones at different pore pressure).

$$\mathbf{v} = \begin{pmatrix} v_x \\ v_z \end{pmatrix} = i\omega \Bigg[U_P^- \begin{pmatrix} \beta_P \\ -\gamma_P \end{pmatrix} \exp(i\omega s_P z) + U_S^- \begin{pmatrix} \beta_S \\ -\gamma_S \end{pmatrix} \exp(i\omega s_S z) \times U_P^+ \begin{pmatrix} \beta_P \\ \gamma_P \end{pmatrix} \exp(-i\omega s_P z) + U_S^+ \begin{pmatrix} \beta_S \\ \gamma_S \end{pmatrix} \times \exp(-i\omega s_S z) \Bigg] \exp[i\omega(t - sx)], \tag{A-1}$$

where ω is the frequency, t is the time variable, U^- are upgoing-wave amplitudes, U^+ are downgoing-wave amplitudes, and

$$\beta = \left[\frac{c_{55}s^2 + c_{33}s_z^2 - \rho}{c_{11}s^2 + c_{33}s_z^2 + c_{55}(s^2 + s_z^2) - 2\rho} \right]^{1/2} \tag{A-2}$$

and

$$\gamma = \pm \left[\frac{c_{11}s^2 + c_{55}s_z^2 - \rho}{c_{11}s^2 + c_{33}s_z^2 + c_{55}(s^2 + s_z^2) - 2\rho} \right]^{1/2}. \tag{A-3}$$

The signs + and − correspond to the qP- and qS-waves, respectively, and s_z is the vertical complex slowness, equal to s_P for qP-waves and to s_S for qS-waves. Moreover, β and γ are the horizontal and vertical complex polarizations, respectively (see, for instance, Carcione, 1997). The slowness relation

(Carcione, 1997) is solved for s_z, given the horizontal slowness s. It yields

$$s_z = \pm\frac{1}{\sqrt{2}}\left(K_1 \mp \sqrt{K_1^2 - 4K_2K_3}\right)^{1/2}, \tag{A-4}$$

where

$$K_1 = \rho\left(\frac{1}{c_{55}} + \frac{1}{c_{33}}\right) + \frac{1}{c_{55}}\left[\frac{c_{13}}{c_{33}}(c_{13} + 2c_{55}) - c_{11}\right]s^2,$$

$$K_2 = \frac{1}{c_{33}}\left(c_{11}s^2 - \rho\right), \quad K_3 = s^2 - \frac{\rho}{c_{55}}.$$

The signs are assigned as follows: (+,−): downward qP-wave; (+,+): downward qS-wave; (−,−): upward qP-wave; (−,+): upward qS-wave [the first signs are explicitly given in equation (A-1)].

Normal stresses σ and strains are related by

$$i\omega\sigma_{zz} = c_{13}v_{x,x} + c_{33}v_{z,z}, \quad i\omega\sigma_{xz} = c_{55}(v_{x,z} + v_{z,x}) \tag{A-5}$$

(e.g., Carcione, 1997). Using equations (A-1) and (A-5), the velocity-stress vector, inside the layer at depth z, can be written as

$$\mathbf{t}(z) = \begin{pmatrix} v_x \\ v_z \\ \sigma_{zz} \\ \sigma_{xz} \end{pmatrix} = \mathbf{T}(z)\begin{pmatrix} U_P^- \\ U_S^- \\ U_P^+ \\ U_S^+ \end{pmatrix}, \tag{A-6}$$

where

$$\mathbf{T}(z) = i\omega\begin{pmatrix} \beta_P & \beta_S & \beta_P & \beta_S \\ -\gamma_P & -\gamma_S & \gamma_P & \gamma_S \\ -Z_P & -Z_S & -Z_P & -Z_S \\ W_P & W_S & -W_P & -W_S \end{pmatrix} \times \begin{pmatrix} e^{i\omega s_P z} & 0 & 0 & 0 \\ 0 & e^{i\omega s_S z} & 0 & 0 \\ 0 & 0 & e^{-i\omega s_P z} & 0 \\ 0 & 0 & 0 & e^{-i\omega s_S z} \end{pmatrix}, \tag{A-7}$$

with

$$W = c_{55}(\gamma s + \beta s_z) \quad \text{and} \quad Z = \beta c_{13}s + \gamma c_{33}s_z. \tag{A-8}$$

As before, the signs corresponding to the propagation directions are explicitly given in equation (A-7). Then, the fields at $z = 0$ and $z = h$ are related by the following equation:

$$\mathbf{t}(0) = \mathbf{B}\,\mathbf{t}(h), \qquad \mathbf{B} = \mathbf{T}(0)\mathbf{T}^{-1}(h), \tag{A-9}$$

which plays the role of a boundary condition. Note that when $h = 0$, $\mathbf{B}$ is the identity matrix.

Let us denote by the subscript 1 the upper half-space and by the subscript 2 the lower half-space. Moreover, the subscripts I, R, and T denote the incident, reflected, and transmitted waves, respectively. Using symmetry properties to define the polarization of the reflected waves, the particle velocities for a P-wave incident from above the layer are given by

$$\mathbf{v}_1 = \mathbf{v}_{P_I} + \mathbf{v}_{P_R} + \mathbf{v}_{S_R}, \tag{A-10}$$

$$\mathbf{v}_2 = \mathbf{v}_{P_T} + \mathbf{v}_{S_T}, \tag{A-11}$$

where

$$\mathbf{v}_{P_I} = i\omega\left(\beta_{P_1}, \gamma_{P_1}\right)^\top \exp\left[i\omega\left(t - sx - s_{P_1}z\right)\right], \tag{A-12}$$

$$\mathbf{v}_{P_R} = i\omega R_{PP}\left(\beta_{P_1}, -\gamma_{P_1}\right)^\top \exp\left[i\omega\left(t - sx + s_{P_1}z\right)\right], \tag{A-13}$$

$$\mathbf{v}_{S_R} = i\omega R_{PS}\left(\beta_{S_1}, -\gamma_{S_1}\right)^\top \exp\left[i\omega\left(t - sx + s_{S_1}z\right)\right], \tag{A-14}$$

$$\mathbf{v}_{P_T} = i\omega T_{PP}\left(\beta_{P_2}, \gamma_{P_2}\right)^\top \exp\left[i\omega\left(t - sx - s_{P_2}z\right)\right], \tag{A-15}$$

$$\mathbf{v}_{S_T} = i\omega T_{PS}\left(\beta_{S_2}, \gamma_{S_2}\right)^\top \exp\left[i\omega\left(t - sx - s_{S_2}z\right)\right], \tag{A-16}$$

where

$$\begin{pmatrix} \beta_P \\ \gamma_P \end{pmatrix} = \frac{1}{\sqrt{s^2 + s_P^2}}\begin{pmatrix} s \\ s_P \end{pmatrix}, \begin{pmatrix} \beta_S \\ \gamma_S \end{pmatrix} = \frac{1}{\sqrt{s^2 + s_S^2}}\begin{pmatrix} s_S \\ -s \end{pmatrix}, \tag{A-17}$$

with

$$s^2 + s_{P_i}^2 = \frac{\rho_i}{E_i} \equiv \frac{1}{V_{P_i}^2}, \quad s^2 + s_{S_i}^2 = \frac{\rho_i}{\mu_i} \equiv \frac{1}{V_{S_i}^2}, \quad i = 1, 2, \tag{A-18}$$

where V_{P_i} and V_{S_i} are the complex compressional and shear velocities, respectively. On the other hand, the W and Z coefficients for the isotropic half-spaces are

$$W_{P_i} = 2\mu_i s_{P_i} s V_{P_i}, \quad W_{S_i} = \mu_i\left(s_{S_i}^2 - s^2\right)V_{S_i}, \tag{A-19}$$

$$Z_{P_i} = \left(\lambda_i s^2 + E_i s_{P_i}^2\right)V_{P_i}, \quad Z_{S_i} = -2\mu_i s_{S_i} s V_{S_i}, \tag{A-20}$$

where $\lambda_i = E_i - 2\mu_i$ and μ_i are complex Lamé constants. Using equations (A-10) and (A-12)–(A-16), the velocity-stress field at $z = 0$ can be expressed as

$$\mathbf{t}(0) = \mathbf{A}_1\mathbf{r} + \mathbf{i}_P, \tag{A-21}$$

where

$$\mathbf{r} = \left[R_{PP}, R_{PS}, T_{PP}, T_{PS}\right]^\top, \tag{A-22}$$

$$\mathbf{i}_P = i\omega\left[\beta_{P_1}, \gamma_{P_1}, -Z_{P_1}, -W_{P_1}\right]^\top, \tag{A-23}$$

and

$$\mathbf{A}_1 = i\omega\begin{pmatrix} \beta_{P_1} & \beta_{S_1} & 0 & 0 \\ -\gamma_{P_1} & -\gamma_{S_1} & 0 & 0 \\ -Z_{P_1} & -Z_{S_1} & 0 & 0 \\ W_{P_1} & W_{S_1} & 0 & 0 \end{pmatrix}. \tag{A-24}$$

On the other hand, using equations (A-11) and (A-12)–(A-16), the velocity-stress field at $z = h$ can be expressed as

$$\mathbf{t}(h) = \mathbf{A}_2\mathbf{r}, \tag{A-25}$$

where

$$\mathbf{A}_2 = i\omega \begin{pmatrix} 0 & 0 & \beta_{P_2}\exp(-i\omega s_{P_2}h) & \beta_{S_2}\exp(-i\omega s_{S_2}h) \\ 0 & 0 & \gamma_{P_2}\exp(-i\omega s_{P_2}h) & \gamma_{S_2}\exp(-i\omega s_{S_2}h) \\ 0 & 0 & -Z_{P_2}\exp(-i\omega s_{P_2}h) & -Z_{S_2}\exp(-i\omega s_{S_2}h) \\ 0 & 0 & -W_{P_2}\exp(-i\omega s_{P_2}h) & -W_{S_2}\exp(-i\omega s_{S_2}h) \end{pmatrix}. \tag{A-26}$$

Combining equations (A-9), (A-21), and (A-25) yields a matrix equation for the reflection and transmission coefficient vector $\mathbf{r}$:

$$(\mathbf{A}_1 - \mathbf{B}\mathbf{A}_2)\mathbf{r} = -\mathbf{i}_P. \tag{A-27}$$

The reflection and transmission coefficients R_{SP}, R_{SS}, T_{SP}, and T_{SS} for an incident S-wave have the same scattering matrix as the incident P-wave, but the vector $\mathbf{i}_P$ is replaced by

$$\mathbf{i}_S = i\omega\left[\beta_{S_1}, \gamma_{S_1}, -Z_{S_1}, -W_{S_1}\right]^\top. \tag{A-28}$$

It is straightforward to generalize this approach for computing the seismic response of a stack of anisotropic layers. I consider N layers with stiffnesses $c_{IJ\alpha}$, density ρ_α, each of them with thickness h_α, such that the total thickness is $h = \sum_{\alpha=1}^{N} h_\alpha$. Matching boundary conditions at the interfaces between layers, it is easy to show that the matrix system giving the reflection and transmission coefficients has the form (A-27) with

$$\mathbf{B} = \prod_{\alpha=1}^{N} \mathbf{B}_\alpha, \quad \mathbf{B}_\alpha = \mathbf{T}(0)\mathbf{T}^{-1}(h_\alpha), \quad \alpha = 1, \ldots, N. \tag{A-29}$$

This recursive approach, which is the base of most reflectivity algorithms, dates back to Thomson (1950), and is illustrated by Brekhovskikh (1960, p. 61) for a stack of isotropic and elastic layers.